Journal of Marine Science and Technology

Volume 27 | Issue 2 Article 4

SPECTRAL ANALYSIS OF TRAIN-RAIL-BRIDGE COUPLING SYSTEM CONSIDERING FREQUENCY-DEPENDENT STIFFNESS OF RAIL FASTENING SYSTEMS

Linya Liu
Engineering Research Center of Railway Environment Vibration and Noise, Ministry of Education, East China Jiaotong University, Nanchang, China

Jialiang Qin
Engineering Research Center of Railway Environment Vibration and Noise, Ministry of Education, East China Jiaotong University, Nanchang, China

Quanmin Liu
Engineering Research Center of Railway Environment Vibration and Noise, Ministry of Education, East China Jiaotong University, Nanchang, China.

Jong-Dar Yau
Department of Architecture, Tamkang University, New Taipei City, Taiwan, R.O.C., jdyau@mail.tku.edu.tw

Rui Song
Engineering Research Center of Railway Environment Vibration and Noise, Ministry of Education, East China Jiaotong University, Nanchang, China

Recommended Citation

Liu, Linya; Qin, Jialiang; Liu, Quanmin; Yau, Jong-Dar; and Song, Rui (2019) "SPECTRAL ANALYSIS OF TRAIN-RAIL-BRIDGE COUPLING SYSTEM CONSIDERING FREQUENCY-DEPENDENT STIFFNESS OF RAIL FASTENING SYSTEMS," *Journal of Marine Science and Technology*: Vol. 27 : Iss. 2 , Article 4.
DOI: 10.6119/JMST.201904_27(2).0004
Available at: https://jmstt.ntou.edu.tw/journal/vol27/iss2/4

SPECTRAL ANALYSIS OF TRAIN-RAIL-BRIDGE COUPLING SYSTEM CONSIDERING FREQUENCY-DEPENDENT STIFFNESS OF RAIL FASTENING SYSTEMS

Acknowledgements

The partial work reported herein is supported by National Natural Science Foundation of China (Grant Nos. 51578238) and the Ministry of Science & Technology of Taiwan via the grant numbers (MOST 107-2221-E-032-002-MY2, 106-2923- E-002-007-MY3). Such financial supports to the present research are gratefully acknowledged.

Journal of Marine Science and Technology, Vol. 27, No. 2, pp. 114-122 (2019)
DOI: 10.6119/JMST.201904_27(2).0004

SPECTRAL ANALYSIS OF TRAIN-RAIL-BRIDGE COUPLING SYSTEM CONSIDERING FREQUENCY-DEPENDENT STIFFNESS OF RAIL FASTENING SYSTEMS

Linya Liu[1], Jialiang Qin[1], Quanmin Liu[1], Jong-Dar Yau[2], and Rui Song[1]

Key words: dynamic flexibility method, frequency-dependent stiffness, rail fastening system; rail-pad, train-rail-bridge system.

ABSTRACT

A rubber rail-pad is typically inserted between the rail and the sleeper to attenuate wheel/rail vibrations for conventional train-rail-bridge (TRB) system. For mathematical modeling, a rail-fastener with rubber pad is simplified as a spring-dashpot unit, whose spring stiffness is related to the exciting frequency of external loads. To exhibit such characteristics of rail-pads on TRB dynamics, based on dynamic flexibility method, two computational models of constant/frequency-dependent stiffness (FDS) are considered for comparison. Numerical studies reveal that the FDS model provides a strengthening benefit for the wheel-rail vibration, from which the shifted dominant frequencies in spectral response are observed.

I. INTRODUCTION

Express intercity transport plays a key role to raise economic development of modern cities in China. However, the vibration and noise radiation caused by a train moving on bridges may result in significant environmental impacts along railway lines (Crockett and Pyke, 2000; Schulte-Werning et al., 2006; Xu and Wu, 2012). To reduce such environmental vibration problems, inserting rubber rail-pads between the sleeper and the rail, as shown in Fig. 1, is a typical method for ballasted/non-ballasted tracks, in which the fastener and the rubber rail-pad constitute a rail-fastening unit, as shown in Figs. 1(b) and 1(c). According to previous studies (Fenander, 1997; Thompson and Verheij, 1997; Maes and Guillaume, 2006), the fastening stiffness of rail-fasteners depends upon the dynamic properties of the rail-pads. Considering the frequency-dependent characteristics of dynamic stiffness for the rail-fasteners, Wang and co-workers (Wang et al., 2015; 2016a, b) carried out a series of experimental and numerical researches on dynamic interaction of wheel-rail system. They integrated the symplectic method and the pseudo-excitation method (2017a; 2017b) to study the random vibration of vehicle-rail and vehicle-rail-tunnel coupling systems, respectively. Combining the vehicle-track coupled dynamics with acoustic propagation theory, Yin et al. (Yin et al., 2017) conducted the wheel-rail noise radiation analysis for a train-rail system, for

(a) non-ballasted slab track

(b) rail fastening device

(c) rail-pad with rubber material

Fig. 1. Photos of rail-pads and fasteners resting on slab-track.

Paper submitted 22/09/18; revised 08/02/19; accepted 26/02/19. Author for correspondence: Jong-Dar Yau (e-mail: jdyau@mail.tku.edu.tw).
[1] *Engineering Research Center of Railway Environment Vibration and Noise, Ministry of Education, East China Jiaotong University, Nanchang, China.*
[2] *Department of Architecture, Tamkang University, New Taipei City, Taiwan, R.O.C.*

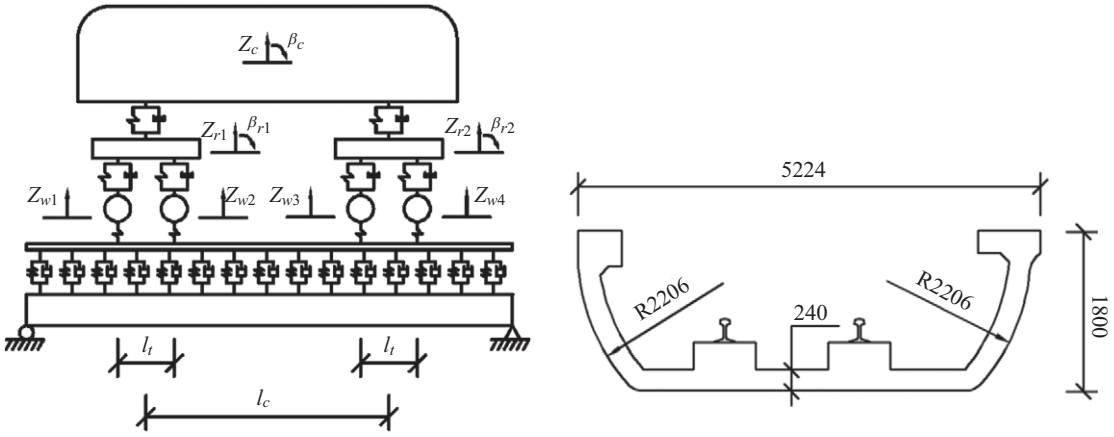

(a) planar TRB coupling system (b) channel section of the rail-bridge

Fig. 2. Schematic model of a train-rail-bridge system.

which the frequency-dependent stiffness of rail-pads was accounted. However, in most of these studies, the frequency-dependent properties of dynamic stiffness in a rail-fastening unit were not completely taken into consideration in response analysis of a train-rail-bridge (TRB) coupling system for urban metro system. Since the dynamic interaction analysis of a TRB system is related to complicated computational procedures in dealing with coupled system dynamics using conventional dynamic stiffness methods. Hence, this study proposed an alternative of dynamic flexibility method to investigate the dynamic response of the TRB system, in which the nature of frequency-dependent stiffness of rail-fasteners is accounted for spectral response analysis. The present results indicated that the dominant frequency of spectral acceleration response in wheel-rail contact of the TRB system would be shifted to higher ones once the dynamic characteristics of frequency-dependent stiffness of the rubber rail-pads are taken into account in performing TRB coupling analysis. Such a strengthening benefit can be used to mitigate the intensive vibration between the wheel-rail and slab-track system through the viscous nature of rubber rail-pads.

II. DYNAMIC FLEXIBILITY OF THE TRB SYSTEM

In this paper, the dynamic model of TRB system is employed to simulate the train-induced vibration of viaducts in urban-metro system. As shown in Fig. 2, a multi-body coach with primary and secondary suspension systems is modeled as a rigid car-body supported by two bogies with four wheel-sets, the rail is regarded as a Timoshenko beam resting on bridge deck and the bridge as a simply supported Bernoulli-Euler beam, in which the discrete rail-pad/fastener units fastening the rails on concrete slabs are simplified as a series of spring-dashpot units with equal intervals (see Fig. 2(a)). Moreover, the equivalent linear Hertzian contact theory is adopted to describe the contact relation between the moving wheel and the stationary rail (Lei, 2015) because of low operating speeds in urban metro system. For conventional structural dynamic analysis, displacement-based stiffness method is a popular approach to formulate the structural matrices by finite element (FE) modeling for response analysis. However, the dynamic stiffness method may encounter a difficulty in accurately predicting higher mode frequencies (ω) since the structural stiffness proportionally increases with ω^2 of a dynamic system. In contrast, the force-based flexibility method has relative robustness to affect the high mode frequencies of a structure because it rapidly decreases with $1/\omega^2$ (Gao and Spencer, 2002). Hence, this study adopted the dynamic flexibility method for coupled dynamic analysis of a TRB system. First, the whole TRB system is divided into two subsystems, i.e., the coach model and the rail-bridge system. Then the spectral response analysis of the TRB system with/without considering frequency-dependent stiffness of the rubber rail pads is carried out to assess the vibration levels of the TRB's components.

1. Dynamic Flexibility Matrix of the Coach Model

To predict the dynamic response of a vehicle moving on a bridge accurately, a number of complicated vehicle-bridge interaction (VBI) models based on FE method were proposed to assess the manipulation and riding comfort of a train moving on a bridge (Yang et al., 2004; Yau 2004; Wang et al., 2013; Lei 2015; Yau et al., 2016). However, solving the coupled equations of motion for a TRB system in temporal domain needs much CPU time in numerical computations. To simplify the complicated computations, the entire TRB system is decomposed into the coach and rail-bridge subsystems, connected by linear Hertz's spring. These two subsystems are first analyzed by dynamic flexibility method individually and then coupled through the enforcing conditions of force equilibrium and deformation compatibility (Raghavan and Srikantha-Phani, 2015).

Considering the planar coach model shown in Fig. 2, the simplified multi-body model is composed by one rigid car-body supported by two bogies with four wheel-sets, where the symbol

l_c is denoted as the interval between two bogies and l_t the length between two wheel-sets of a bogie. The dynamic response $\{Z_V(t)\}$ of the coach can be described by the following matrix equation as:

$$\left[M_v\right]\left\{\ddot{z}_V(t)\right\}+\left[C_v\right]\left\{\dot{z}_V(t)\right\}+\left[K_v\right]\left\{z_V(t)\right\}=\left\{p(t)\right\} \quad (1)$$

where ($[M_V]$, $[C_V]$, $[K_V]$) represent the mass, damping and stiffness matrices of the coach model, respectively, $\{Z_V(t)\}$ the displacement vector of the coach, $\{p(t)\}$ the contact force vector between the wheel-sets and the rails, which are related to the track irregularities and beam deflections. Thus one can transform the differential equations in temporal domain of Eq. (1) into the following spectral matrix equation

$$\left(-\omega^2\left[M_v\right]+i\omega[C_v]+[K_V]\right)\left\{Z_V(\omega)\right\}=\left\{p(\omega)\right\} \quad (2)$$

here, ω is denoted as the exciting frequency due to random irregularity, $\{P(\omega)\}$ the spectral amplitude vectors of the contact force and $\{Z_V(\omega)\}$ the vehicle's response. By solving the spectral displacement response of $\{Z_V(\omega)\}$ from Eq. (2), the flexibility coefficient $\left(\beta_{ij}^V\right)$ of the i-th wheel-set of the railcar model moving at the j-th position on the rail can be obtained, from which the dynamic flexibility coefficient matrix is expressed as:

$$\boldsymbol{\beta}^{\mathbf{V}}=\left[\beta_{ij}^V\right]=\left[Z_{ij}^V/P_j\right],\quad i,j=1,2,3,4 \quad (3)$$

where Z_{ij}^V represents the displacement response of the i-th wheel-set moving on the j-th contact point of the rail, P_j the corresponding contact force of the wheel-set and $\boldsymbol{\beta}^{\mathbf{V}}$ the corresponding dynamic flexibility matrix of the coach model.

2. Dynamic Flexibility Matrix of the Rail-Bridge Sub-System

As shown in Fig. 2, the rail-bridge subsystem is modeled as an infinitely long Timoshenko beam resting on the simply supported beam connected by a series of rail-pad/fastener units with identical intervals, in which the rail-pad/fastener is modeled as an equivalent spring-dashpot unit and the elastic bearings supporting the beam structure at two ends on bridge piers are idealized as set of equivalent spring bearings. Then the dynamic displacement at x_1 of the Timoshenko beam subject to a harmonic load at x_2 is given as (Thompson and Verheij, 1997)

$$\beta_r(x_1,x_2)=u_1e^{-ik_1|x_1-x_2|}+u_2e^{-ik_2|x_1-x_2|} \quad (4)$$

where $\beta_r(x_1, x_2)$ represents the displacement at the point of x_1 caused by a unit harmonic load acting on the position x_2 of the rail and the dynamic coefficients of (k_1, k_2) and the amplitudes of (u_1, u_2) are respectively given as follows:

$$k_{1,2}\left(\frac{\omega}{\sqrt{2}}\right)\left\{\pm\left(\frac{\rho_r}{E_r\left(1+i\eta_r\right)}+\frac{\rho_r}{\kappa G_r\left(1+i\eta_r\right)}\right)+\left[\left(\frac{\rho_r}{E_r\left(1+i\eta_r\right)}-\frac{\rho_r}{\kappa G_r\left(1+i\eta_r\right)}\right)^2+\frac{4\rho_rA_r}{E_r\left(1+i\eta_r\right)I_r\omega^2}\right]^{1/2}\right\}^{1/2} \quad (5)$$

$$u_1=\frac{i}{2\kappa G_rE_rI_rA_r\left(1+i\eta_r\right)^2}\frac{\rho_rI_r\omega^2-\kappa G_rA_r\left(1+i\eta_r\right)-E_rI_r\left(1+i\eta_r\right)k_1^2}{k_1\left(k_1^2+k_2^2\right)} \quad (6)$$

$$u_2=\frac{1/\left(1+i\eta_r\right)^2}{2\kappa G_rA_rE_rI_r}\frac{\rho_rI_r\omega^2-\kappa G_rA_r\left(1+i\eta_r\right)-E_rI_r\left(1+i\eta_r\right)k_2^2}{k_2\left(k_1^2+k_2^2\right)} \quad (7)$$

Here, E_r = elastic modulus, G_r = shear modulus, A_r = cross-sectional area, I_r = cross sectional moment of inertia, κ = shear coefficient, ρ_r = density and η_r = loss factor of the rail, respectively.

By using the dynamic flexibility method and the superposition principle, the spectral displacement response of the rail is expressed by Eq. (4) as (Dai et al., 2014)

$$z_r(x,\omega)=\sum_{k=1}^{N_w}\beta_r\left(x,x_k\right)P_k(\omega)-\sum_{n=1}^{N_r}\beta_r\left(x,x_n\right)F_{fn}(\omega) \quad (8)$$

where P_k is the wheel-rail contact force of the k-th wheel-set moving at the position x_k on the rail, N_w the total number of wheel-sets, and F_{fn} the restoring force of the j-th rail-fastener at the position x_n on the rail, and N_r is the total number of fasteners under the rail. Similarly, for a simply supported Bernoulli-Euler beam, the dynamic flexibility of the beam reads (Thompson and Verheij, 1997).

$$\beta_b\left(x_2,x_1\right)=\sum_{n=1}^{NMB}\frac{W_{bn}\left(x_2\right)W_{bn}\left(x_2\right)}{\left(1+i\eta_b\right)\omega_{bn}^2-\omega^2} \quad (9)$$

$$W_{bn}(x)=\sqrt{\frac{2}{\rho_bA_bL_b}}\sin\frac{n\pi x}{L_b},\ \omega_{bn}=\left(\frac{n\pi}{L_b}\right)^2\sqrt{\frac{E_bI_b}{m_b}} \quad (10a, b)$$

where W_{bn} is denoted as the n -th natural mode of a simple beam, ω_{bn} the n-th modal frequency and NMB the total mode number for dynamic analysis of the beam. In addition, the following symbols are used in Eqs. (9) and (10): L_b = span length, E_bI_b = flexural rigidity of the cross section and m_b = mass per length of the beam. Following a similar process, the spectral deflection (z_b) of the beam can be described by Eq. (9) as

$$z_b(x,\omega)=\sum_{n=1}^{N}\beta_b(x,x_n)F_{fn}(\omega)-\sum_{k=1}^{2}\beta_b(x,x_{zk})F_{zk}(\omega) \quad (12)$$

where F_{zk} is denoted as the support reaction of the k-th pad-bearing at the position of x_{zk} on the bridge. With the displacement components of the rail and beam in Eqs. (8) and (12),

respectively, the internal force (F_{fn}) in the rail-fastening unit and the support reaction (F_{zk}) at the supported bearings of the bridge are expressed as:

$$F_{fn} = K_f\left(z_r\left(x_n\right) - z_b\left(x_n\right)\right),\ F_{zk} = K_z z_b\left(x_k\right) \quad (13a, b)$$

here, K_f is denoted as the complex stiffness of the rail-fastener with a loss factor of η_f and K_z as the complex stiffness of the supported spring with a loss factor of η_z, both of which are respectively expressed in complex form as:

$$K_f = k_f(1+i\eta_f),\ K_z = k_z(1+i\eta_z) \quad (14a, b)$$

Let us adopt the relation of force-deformation for a rail-bridge system. The substitution of Eq. (13) into Eqs. (8) and (12), respectively, yields the following simultaneous equations

$$\begin{aligned} &z_r(x) + \sum_{n=1}^{N}\beta_r\left(x, x_n\right)K_{fn}z_r\left(x_n\right) \\ &\quad - \sum_{n=1}^{N}\beta_b\left(x, x_n\right)K_{fn}z_b\left(x_n\right) = \sum_{w=1}^{Nw}\beta_r\left(x, x_w\right)P_w \\ &z_b(x) - \sum_{n=1}^{N}\beta_b\left(x, x_n\right)K_{fn}z_r\left(x_n\right) \\ &\quad + \sum_{n=1}^{N}\beta_b\left(x, x_n\right)K_{fn}z_b\left(x_n\right) \\ &\quad + \sum_{k=1}^{2}\beta_b\left(x, x_n\right)K_{zk}z_b\left(x_k\right) = 0 \end{aligned} \quad (15a, b)$$

For simplified expression, Eqs. 15(a) and 15(b) can be written using the following matrix equation as:

$$\left[\mathbf{K}_{\boldsymbol{\beta}}\right]\{\mathbf{Z}\} = \{\mathbf{P}\} \quad (16)$$

where $[\mathbf{K}_{\boldsymbol{\beta}}]$ represents the dynamic complex stiffness matrix, $[\mathbf{Z}]$ the response vector of the rail-bridge system and $\{\mathbf{P}\}$ the load vector. Following the similar derivation process of dynamic flexibility shown in Eq. (3), the solution of Eq. (16) yields the dynamic flexibility matrix of the rail-bridge system, that is,

$$\boldsymbol{\beta}^{\mathbf{TB}} = \left[\beta_{ij}^{TB}\right]_{4\times4} = \left[Z_{ij}^{TB}/P_j\right],\quad i, j = 1, 2, 3, 4 \quad (17)$$

here, β_{ij}^{TB} represents the spectral displacement response of the rail at the i-th contact point with the contact force P_j moving on the j-th position of the rail, β_{ij}^{TB} the corresponding dynamic flexibility coefficient and $\boldsymbol{\beta}^{\mathbf{TB}}$ the 4×4 dynamic flexibility matrix of the rail-bridge system.

3. Dynamic Flexibility of the Linear Hertzian spring

The nonlinear contact stiffness of wheel-rail sysem is related to not only the wheel/rail contact force but also the shape of the wheel and rail-tread (Lei, 2015). As a wheel is rolling on a straight track, the nonlinear Hertzian contact relation between two cylinders (Zhai, 2015; Wei et al., 2016c) is adopted to describe the vertical contact between the wheel and the rail, that is,

$$y = Gp^{2/3} \quad (18)$$

where y is the relative displacement between the wheel and the rail in contact, p the wheel-rail contact force and G the interference coefficient. Depending on the thread types of the rolling wheel on the rail, the interference coefficient G is given by:

$$\text{For a tapered tread: } G = 4.57R^{-0.149}\times10^{-8} \quad (19a)$$

$$\text{For a wear-type tread: } G = 3.86R^{-0.115}\times10^{-8} \quad (19b)$$

here, R represents the radius of the wheel. To formulate the equivalent stiffness of Hertzian spring between the wheel and rail, the equation of Eq. (18) can be rewritten as

$$p = \frac{1}{G^{3/2}}y^{3/2} = Cy^{3/2} \quad (20)$$

where $C = 1/G^{3/2}$ is called the contact stiffness of equivalent spring between the wheel and rail. In this study, the wheel-rail contact spring is assumed as an equivalently linearized Hertzian spring. Thus one can approximate the linear stiffness of the nonlinear Hertzian spring as:

$$k_c = \left.\frac{dp}{dy}\right|_{p=p_0} = \frac{3}{2G}p_0^{1/3} \quad (21)$$

where k_c is called the linearized wheel-rail contact stiffness and p_0 the static axle-load acting on the rail. Then the dynamic flexibility matrix ($\boldsymbol{\beta}^{\mathbf{c}}$) of the wheel-rail contact springs for a coach with four axle-loads can be directly formulated using the inverse relation of Eq. (21) as:

$$\boldsymbol{\beta}^{\mathbf{c}} = \begin{bmatrix} 1/k_c & & & \\ & 1/k_c & & \\ & & 1/k_c & \\ & & & 1/k_c \end{bmatrix} \quad (22)$$

4. Response Analysis of the TRB System

Due to the regular axle-arrangement of wheel-sets in the two bogies of a coach, as shown in Fig. 2(a), the rail irregularity under the i-th moving wheel on the rail can be expressed in term of the sequential arriving-time of the wheel in contact with the

rail. Thus, the rail irregularity functions beneath the four wheel-sets can be expressed in a vector form as

$$\mathbf{r}(t) = \left\{ r_1(t-t_1)\ r_1(t-t_2)\ r_1(t-t_3)\ r_1(t-t_4) \right\}^T \qquad (23)$$

here, the irregularity function $r_1(t-t_i)\big|_{i=1\sim4}$ represents the irregularity amplitude beneath the i-th wheel at the arriving-time t_i. Let us consider a typical metro-coach with four axle-loads moving at constant speed V, if the initial time for the first wheel-set is set $t_1 = 0$ then the arrival times of the following three wheel-sets are given: $t_2 = 2l_t/V$, $t_3 = 2l_c/V$ and $t_4 = 2(l_t + l_c)/V$, respectively. Here the intervals of l_t and l_c have been shown on Fig. 2(a).

By the fast Fourier transform (FFT), the vector form of exciting sources induced by irregularities to the TRB system, as shown in Eq. (23) can be expressed in frequency domain as:

$$\mathbf{R}(\omega) = \left\{ 1 \quad e^{-2i\omega l_t/V} \quad e^{-2i\omega l_c/V} \quad e^{-2i\omega(l_t+l_c)/V} \right\}^T r_1(\omega) \qquad (24)$$

here, $r_1(\omega)$ represents the transformed function of the rail irregularity $r(t)$ after FFT. Since the running speed of a train is much smaller than the phase speed of elastic waves propagating in steel rail, the use of track irregularity as an exciting source to a moving train is acceptable for train dynamics. By using the force-equilibrium relation to relate the dynamic flexibility matrices of ($\boldsymbol{\beta}^{\mathbf{V}}$, $\boldsymbol{\beta}^{\mathbf{TB}}$, $\boldsymbol{\beta}^{\mathbf{c}}$) in Eqs. (3), (7) and (17) with the excitation vector of Eq. (24) for the TRB system, one can obtain the dynamic wheel-rail force vector $\mathbf{P_{wr}}$ from the displacement equations as $\mathbf{R}(\boldsymbol{\omega}) = (\boldsymbol{\beta}^{\mathbf{V}} + \boldsymbol{\beta}^{\mathbf{TB}} + \boldsymbol{\beta}^{\mathbf{c}})\mathbf{P_{wr}}$ or

$$\mathbf{P_{wr}} = (\boldsymbol{\beta}^{\mathbf{V}} + \boldsymbol{\beta}^{\mathbf{TB}} + \boldsymbol{\beta}^{\mathbf{c}})^{-1}\mathbf{R}(\boldsymbol{\omega}) \qquad (25)$$

By substituting the wheel-rail force vector $\mathbf{P_{wr}}$ of Eq. (25) into Eqs. (4) and (16), respectively, the spectral responses of the car body ($\{Z_I(\omega)\}$) and rail-bridge system ([**Z**]) are obtained. Then the spectral responses of ($\{Z_I(\omega)\}$, [**Z**]) can be used to evaluate the dynamic performance of the FDS model on vibration analysis of the TRB system.

III. FREQUENCY-DEPENDENT STIFFNESS OF THE RAIL-FASTENING SYSTEM

To investigate the dynamic characteristics of frequency-dependent stiffness of the rail-fastener described in Section 2, the metro-coach A and the channel bridge with non-ballasted tracks (see Fig. 2(b)) in the Nanchang Metro are considered. Tables 1 and 2 listed the properties of the metro-coach A and the channel bridge, respectively. The fundamental frequency of the channel bridge with supported bearings is 6.6 Hz, which approximates the following simplified formula proposed by Yang et al. (2004).

Table 1. Properties of the metro-coach A (Wei et al., 2016b).

Parameter	Value
Car-body mass (t)	46
Bogie mass (t)	4.36
Wheel-set mass (t)	1.77
Pitching moment of inertia of the car-body (t · m^2)	1959
Pitching moment of inertia of the bogie (t · m^2)	1.47
Primary suspension stiffness (kN · m^{-1})	2976
Primary suspension damping s (kN · m^{-1})	15
Secondary suspension stiffness (kN · m^{-1})	1060
Secondary suspension damping s (kN · m^{-1})	30
Vehicle length (m)	22.8
Length between bogie centers (m)	15.625
Rigid wheel base (m)	2.5

Table 2. Properties of the rail-bridge system (Li et al., 2012).

Parts	Item	Value
Rail	Elastic modulus (N/m^2)	2.1e10
	Cross-sectional moment of inertia (N/m^2)	3.217e-5
	Density (kg/m^3)	7850
	Cross-sectional area (m^2)	7.745e-3
	Shear modulus (N/m^2)	7.7e10
	Sectional factor	0.5331
	Loss factor	0.01
Fastener	Spacing (m)	0.625
	Loss factor	0.25
Bridge	Length (m)	30
	Elastic modulus (N/m^2)	3.55e10
	Sectional moment of inertia (m^4)	6.859
	Density (kg/m^3)	2600
	Sectional area (m^2)	2.205
	Loss factor	0.05
Support Bearing	Stiffness (N/m)	2e8
	Support spacing (m)	30
	Loss factor	0.25

$$f_0 = \frac{\omega_0}{2\pi}\sqrt{\frac{\pi + 4\kappa}{\pi + 8\kappa + 2\pi\kappa^2}}$$
$$\text{with } \omega_0 = \left(\frac{\pi}{L}\right)^2\sqrt{\frac{EI}{m}},\ \kappa = \frac{EI\pi^3}{K_b L^3} \qquad (26a\text{-}c)$$

where (EI, L, m) = flexural rigidity, length, and mass/length of the beam, and K_b = supporting stiffness of the bearing.

In this study, the track irregularity graphically plotted in the Chinese High Speed Rail Standard of (GB/T5111-2011, 2011) is adopted and the corresponding irregularity spectrum is fitted using the following linear logarithm function as:

$$20\log_{10}\left(\frac{r}{r_0}\right)=\begin{Bmatrix}18.45\log_{10}\lambda+27.20 & \lambda\geq 0.01\\ -9.70 & \lambda<0.01\end{Bmatrix} \text{ with } \lambda=\frac{2\pi V}{\omega} \tag{27}$$

here, r = central wavelength with amplitude smaller than 0.63 m, r_0 = reference amplitude of rail roughness (= 10^{-6} m), λ = wavelength of one-third frequency interval and ω = exciting frequency.

As a railcar is running on a bridge, the dynamic stiffness of rail-fasteners may change with the exciting frequencies of the wheel-rail system due to the nonlinear stiffness properties of the rubber pads made of Thermoplastic Polyurethane Elastomer (Wei et al., 2016c). From the in-situ experiments in previous literature (Wei et al., 2015; 2016a-c; Liu et al., 2017), the current dynamic stiffness (K) of the rail-fastener and the exciting frequency (f) can be approximated by a linear logarithmic relation as:

$$\log(K)=k\times(\log(f)-\log(f_0))+\log(K_0) \tag{28}$$

where K_0 is the initial stiffness of the rail-pad under low frequency, f_0 the exciting frequency (normally 3-5 Hz) of the wheel-rail system, f the exciting frequency, and k the linear tangential slope of the dynamic stiffness of the rail-fastener to the excitation frequencies of external forces in logarithmic coordinate system. In practice, the linear tangential slope of k is ranged from 0.05 to 0.3 (Maes et al., 2006; Wei et al., 2016c). Here, the positive slope parameter (k) represents the dynamic stiffness of the fastener/rail-pad system rising with the increase of exciting frequency of external loads. Let us observe the linear logarithmic equation of Eq. (28), the frequency-dependent stiffness of rail-pads is not only related to the initial stiffness K_0 in low-frequency but also proportional to the amplitude of the slope parameter k, in which the higher the exciting frequency (f) to the rail-fastener, the more fastening of the connecting stiffness (K) on the rail-fastening unit will be developed. Such a material property provides a strengthening benefit in frequency-dependent stiffness for the rail-fastener to mitigate the intensive vibration between the wheel-rail and the slab-track system in conjunction with the viscous properties of rubber rail-pads. Based on the practical consideration of metro system, the following data are adopted in this study: the exciting frequency f_0 is set 4 Hz and the initial stiffness of the rail-fastener K_0 = 40 kN/mm, and the slope parameter k (= 0.1306) is referred to as the experimental parameters suggested by Maes et al. (2006).

IV. NUMERICAL ILLUSTRATIONS

A convenient way to understand the dynamic behaviors of a structure under external excitations is to obtain its spectral response in frequency domian, from which one can identify the dominant frequency and vibration information of the structure. To evaluate the vibration levels of the TRB system, the frequency distribution of structural response is divided into three levels, i.e., the frequency-band in 1~10 Hz is defined as "low frequency", 10~60 Hz as "medium frequency" and 60~200 Hz as "high frequency" (Wei et al., 2016a; 2016b).

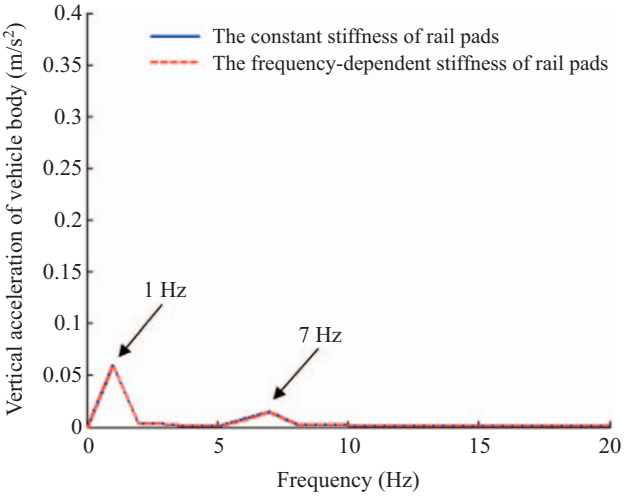

Fig. 3. Vertical acceleration spectrum of the car-body.

Since the influence of frequency-dependent stiffness of rail-fasteners on the spectral response of the TRB system is of concern, the case of one metro coach moving on a channel-bridge with constant speed of 80 km/h is considered in this study. Tables 1 and 2 list the properties of the coach and rail-bridge system in Nanchang Metro. By the response analysis based on dynamic flexibility method described in Sections 2 and 3, the plots of vertical spectral acceleration response vs. frequency at midpoint of the car-body, wheel-set, bogie, and rail-bridge system have been shown in Figs 3-7, respectively. For comparisons, the initial constant stiffness (K_0) of the rail-pad in the rail-fastener is regarded as a reference level to assess the spectral response of the TRB system considering nonlinear frequency-dependent stiffness of the rail-pad. Moreover, two computational models of the rail-fastening system, i.e., the constant stiffness (CS) and the frequency-dependent stiffness (FDS), are considered for numerical investigations. For convenient description, they are denoted as "CS model" and "FDS model" in the following examples, respectively.

1. Spectral Response of the Car-Body

Fig. 3 shows the spectral acceleration response of the car body in low-frequency domain (1~20 Hz). As can be seen, the two response curves, either of which considers the CS or the FDS model to simulate the rail-fastener, are identical and the first peak amplitude takes place at 1 Hz is consistent with the heaving frequency of the car body supported by secondary suspension systems (Wei et al., 2016a, b). As for the second peak amplitude at 7 Hz, it represents the heaving frequency of the bogie to affect the response of the car body. Next, let us observe the magnitudes of the two peak amplitudes at the frequencies of 1 Hz and 7 Hz on Fig. 3, respectively. The results

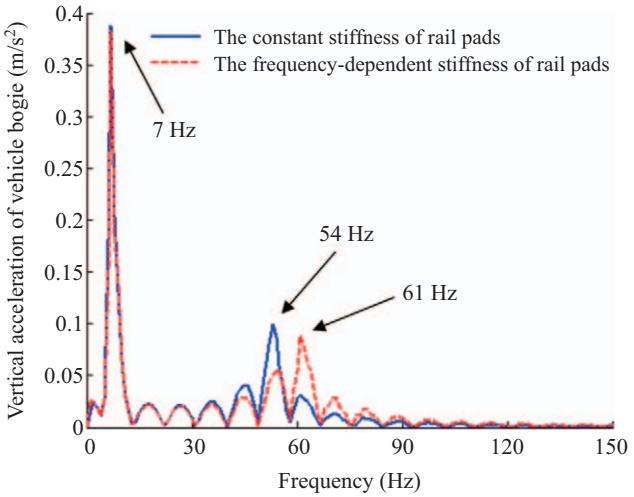

Fig. 4. Vertical acceleration spectrum of the bogies.

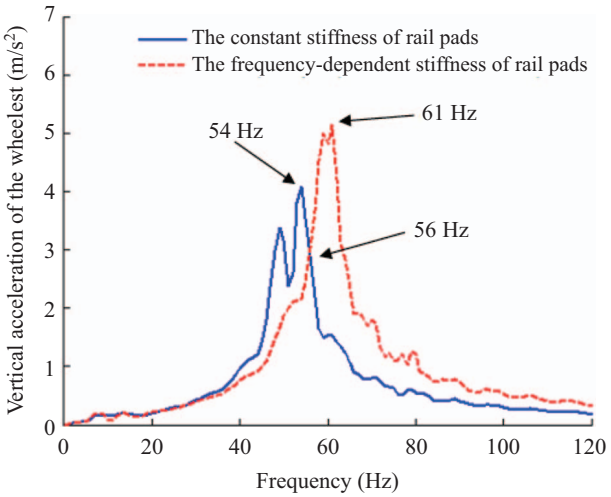

Fig. 5. Vertical acceleration spectrum of the first wheel-set.

indicated that the effects of FDS model on the spectral acceleration of the car-body is negligible due to low-stiffness secondary suspension systems for keeping riding comfort of passengers in a moving metro car. Hence, the smaller peak response in low frequency of the car body does not result in significant noise radiation and vibration near the surroundings along railway lines.

2. Spectral Response of the Bogies

In this example, the vertical acceleration response of the bogies supporting the car body is of interest. From the plot of peak acceleration amplitude vs. frequency shown in Fig. 4, few points are observed:

(a) The first dominant frequency still takes place at 7 Hz with identical peak amplitude for both of the CS and FDS models;
(b) The second peak amplitudes in the two response curves represent the dominant frequencies caused by the wheel-rail in contact. As indicated, the peak amplitude at 54 Hz of the CS model has been shifted to 61 Hz if the FDS model is considered for the rail-fastener. Such a stiffening phenomenon explains why the frequency-dependent stiffness of a rubber rail-pad should be accounted in high-frequency range (57-120 Hz) for vibration evaluation;
(c) In the medium frequency band ranged from 24 Hz to 56 Hz, the peak amplitudes obtained from the FDS model are generally less than those by the CS. However, the difference between them has an increasing trend as the frequency increases in Fig. 4, especially for the peak amplitude at the frequency of 54 Hz due to the wheel-rail contact. Obviously, the FDS model plays a strengthening role in the spectral response of the bogie at medium-frequency;
(d) For the high frequency-band ranged from 57 Hz to 120 Hz, the peak amplitudes of the CS model are less than those of the FDS from 56 Hz. For example, there exists a significant difference of 35% at 61 Hz between them, as explained in Point (b).

3. Spectral Response of the Wheel-Sets

Fig. 5 shows the vertical spectral acceleration response of the first wheel-set. Obviously, the response amplitudes plotted in Fig. 5 are significantly larger than the other results obtained from the coach and bridge system since the wheel-rail in contact is the major exciting source of vibration and noise of the whole TRB system. According to the distribution of peak amplitudes in spectral response curves shown in Fig. 5, four observations are addressed:

(a) The peak spectral acceleration responses of the wheel-set for both computational models are concentrated in the medium frequency-band (40~80 Hz);
(b) The peak amplitude (= 4.087 m/s^2) at the dominant frequency of 54 Hz for the case of the CS model is significant less than the one (= 5.147 m/s^2) at the high frequency of 61 Hz of the FDS. It means the frequency-dependent stiffness of rubber rail-pad in the rail-fastener should be taken into account in assessing the vibration and noise levels of wheel-sets;
(c) For the frequencies less than 56 Hz in Fig. 5, the response amplitudes obtained from the FDS model are generally smaller than those from the CS. It means that the FDS model can produce a dissipating benefit to mitigate the response of the wheel-set below the medium frequency (56 Hz);
(d) Compared to the results in Fig. 4, the response amplitudes at dominant frequencies are significantly less than those shown in Fig. 5. The reason can be explained that the primary suspension units between the bogie-body and the two wheel-sets can produce dissipating actions on vibration reduction of the moving bogies.

4. Spectral Response of the Rail

Fig. 6 shows the plot of vertical spectral acceleration response

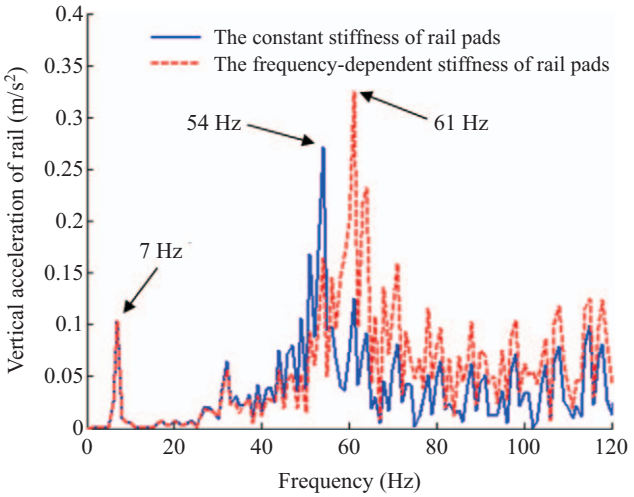

Fig. 6. Vertical acceleration spectrum of the rail.

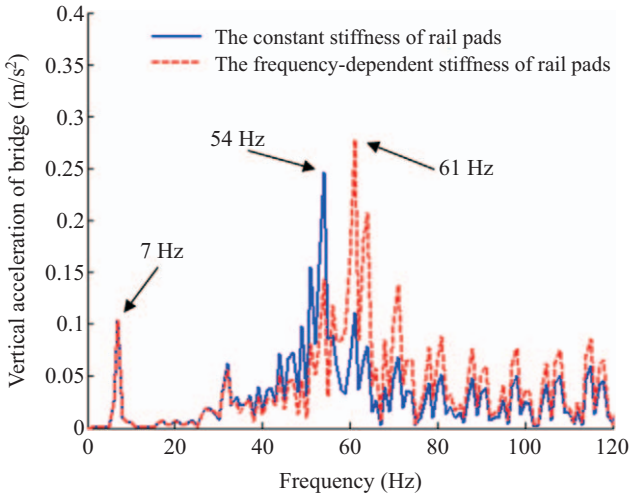

Fig. 7. Vertical acceleration spectrum of the bridge.

of the rail. Since the mass of the bridge is much larger than that of the rails, the rails fastened on the concrete slab of bridge deck would vibrate with the bridge. Hence the first peak at 7 Hz in Fig. 6 is consistent with the vertical modal frequency (6.6 Hz) of the bridge model. For the case of CS model, the peak amplitude of 0.271 m/s^2 occurs at dominant frequency 54 Hz. But for the FDS model, the dominant frequency has been shifted to 61 Hz with a higher amplitude of 0.325 m/s^2. Thus, three points are comprehensively listed as follows:

(a) For the frequencies smaller than 56 Hz, the peak amplitudes obtained from the FDS model are generally smaller than those by the CS. It means that the FDS model play a dissipating role in mitigating the response of the first wheelset in the medium-frequency below 56 Hz;
(b) Once the frequency is larger than 56 Hz, the peak amplitudes obtained by the FDS model are generally larger than those by the CS, in which the dominant frequency has been shifted from 54 Hz to 61 Hz. Such a phenomenon represents that the frequency-dependent stiffness of the FDS model starts activating toward high frequencies;
(c) For the FDS model, increasing dynamic stiffness of the rail-fastening system is helpful to raise energy-dissipating capacity in vibration reduction of the wheel-rail system since the spectral response in high frequency can be efficiently suppressed by viscous damping of rubber rail-pads. This benefit is useful for railway engineers to select a suitable rail-fastening system for vibration reduction of wheel-rail system.

From the present numerical studies, we can conclude that the influence of the FDS model on the spectral accelerations of the car-body and bogie is negligible due to the low-stiffness suspension units. But the spectral acceleration of the rail-wheel system is sensitive to the fastening stiffness of rail-fasteners at high frequency. Thus the frequency-dependent characteristics of dynamic stiffness for the rail-fastening system should be taken into account in assessing vibration levels of wheel-rail system.

5. Spectral Response of the Bridge with Supported Bearings

For the spectral response of the channel-bridge, as shown in Fig. 7, the present results are quite similar to those plotted in Fig. 6 for the rail even the peak amplitudes of the bridge response are slightly less than those of the rail. As expected, the first peak at 7 Hz (or 6.6 Hz) represents the fundamental frequency of the channel bridge. The reason is attributed to (1) the strong fastening effects between the rails and the concrete slab resting on the bridge deck; and (2) the viscous nature of supported bearings at bridge supports. Thus the rails and the bridge appear a synchronous behavior in vibration.

V. CONCLUSIONS

In this study, the spectral response analysis of a TRB coupling system was carried out using dynamic flexibility method, in which the dynamic characteristics of frequency-dependent stiffness in the rail fastening system are accounted for spectral response analysis of the wheel-rail system. In addition to this, few points are concluded as follows:

(1) The influence of the frequency-dependent stiffness of the rail-fastening system on the spectral acceleration response of the car body and bogie in low frequency-range is negligible due to the low-stiffness suspension systems for riding comfort of passenger metro cars;
(2) Considering the frequency-dependent characteristics of dynamic stiffness of rail-pads, the FDS model can provide a strengthening benefit to the dominant frequency in spectral response of the wheel-rail system to higher ones for the TRB system;
(3) In conjunction with the viscous nature of rubber rail-pads, the spectral response at shifted dominant frequency can

be efficiently mitigated for vibration of the wheel-rail and slab-track system.

ACKNOWLEDGEMENTS

The partial work reported herein is supported by National Natural Science Foundation of China (Grant Nos. 51578238) and the Ministry of Science & Technology of Taiwan via the grant numbers (MOST 107-2221-E-032-002-MY2, 106-2923-E-002-007-MY3). Such financial supports to the present research are gratefully acknowledged.

REFERENCES

China National Standardization Management Committee (2011). Acoustic-Measurement of noise emitted by rail bound vehicle (GB/T 5111-2011). Commodity Inspection and Quarantine, Beijing. (in Chinese)

Crockett, A. R. and J. Pyke (2000). Viaduct design for minimization of direct and structure-radiated train noise. Journal of Sound and Vibration 231(3), 883-897.

Dai, F., D. J. Thompson and Y. Zhu (2014). Vibration properties of slab track installed on a viaduct. Proceedings of the Institution of Mechanical Engineers, Part F: Journal of Rail and Rapid Transit 230(1), 9743-9752.

Fenander, A. (1997). Frequency dependent stiffness and damping of railpads. Proceedings of the Institution of Mechanical Engineers, Part F: Journal of rail and Rapid Transit 211(1), 51-62.

Gao, Y., M. Ruiz-Sandoval and B. F. Spencer (2002). Flexibility-based damage localization employing ambient vibration. Proceeding of 15th ASCE Engineering Mechanics Conference, USA.

Lei, X. Y. (2015). High Speed Railway Track Dynamics: Model, Algorithm and Application. Science Press, Beijing. (in Chinese)

Li, Q., Y. L. Xu and D. J. Wu (2012). Concrete bridge-borne low-frequency noise simulation based on vehicle-track-bridge dynamic interaction. Journal of Sound and Vibration 331(10), 2457-2470.

Liu L. Y., J. Qin and F. Zeng (2017). Research on local vibration and parameter sensitivity analysis of rail transit trough beam. Journal of Railway Science and Engineering 14(11), 2363-2368. (in Chinese)

Maes, J., H. Sol and P. Guillaume (2006). Measurements of the dynamic rail pad properties. Journal of Sound and Vibration 293(3), 557-565.

Raghavan, L. and A. Srikantha-Phani (2015). Local resonance band gaps in periodic media: Theory and experiment. The Journal of the Acoustical Society of America 134, 1950-1959.

Schulte-Werning, B., M. Beier and K. G. Degen (2006). Research on noise and vibration reduction at DB to improve the environmental friendliness of railway traffic. Journal of Sound and Vibration 293(3-5), 1058-1069.

Thompson, D. J. and J. W. Verheij (1997). The dynamic behaviour of rail fasteners at high frequencies. Applied Acoustics 52(1), 1-17.

Wang, P., F. Yang and K. Wei (2017a). Symplectic random vibration analysis of vertically coupled vehicle-track-tunnel system considering frequency-dependent stiffness of rail pads. Journal of Southwest Jiaotong University 52(02), 209-215. (in Chinese)

Wang, P., F. Yang and K. Wei (2017b). Symplectic model and its application of vertical environment vibration prediction about vehicle-track-tunnel coupled system. Engineering Mechanics 34(05), 171-178. (in Chinese)

Wang, Y. J., J. D. Yau and Q. C. Wei (2013). Vibration suppression of train-induced multiple resonant responses of two-span continuous bridges using VE dampers. Journal of Marine Science and Technology 21(2), 149-158.

Wei, K., P. Wang and F. Yang (2015). Influence of frequency-dependent dynamic parameters of rail pads on environmental vibration induced by subways in a tunnel. Transportation Research Record: Journal of the Transportation Research Board 2476(1), 8-14.

Wei, K., P. Wang and F. Yang (2016a). The effect of the frequency-dependent stiffness of rail pad on the environment vibrations induced by subway train running in tunnel. Proceedings of the Institution of Mechanical Engineers, Part F: Journal of rail and Rapid Transit 230(3), 171-178.

Wei, K., F. Yang and P. Wang (2016b). Symplectic random vibration analysis of vehicle-track coupled system considering frequency-dependent stiffness of rail pads. Engineering Mechanics 33(09), 123-130. (in Chinese)

Wei, K., P. Zhang, P. Wang, J. Xiao and Z. Luo (2016c). The influence of amplitude- and frequency- dependent stiffness of rail pads on the random vibration of a vehicle-track coupled system. Shock and Vibration http://dx.doi.org/10.1155/2016/7674124, Article ID 7674124.

Yang, J. J. (2015). Study on prediction of high speed vehicle-bridge coupling vibration and viaduct bridge structure noise radiation. Lanzhou Jiaotong University, Lanzhou. (in Chinese)

Yang Y. B., J. D. Yau and Y. S. Wu (2004). Vehicle–Bridge Interaction Dynamics. World Scientific, Singapore.

Yau, J. D. (2004) Vibration of simply supported compound beams to moving loads. Journal of Marine Science and Technology 12(4), 319-328.

Yau, J. D., L. Frýba and S. Urushadze (2016). Seismic response of an arch-beam interacting with sequential moving train loads. Journal of Marine Science and Technology 24(3), 419-425.

Yin, Q., C. B. Cai and S. Y. Zhu (2017). Effect of the frequency-dependent stiffness of rail fasteners on the wheel-rail vibration noise. Journal of Vibration and Shock 36(18), 231-237.

Zhai, W. M. (2015). Vehicle-Track Coupled Dynamics. Science Press, 4rd ed., Beijing. (in Chinese)